Optimization of Silicon Photomultiplier Detectors for Fast Fluorescence Imaging

Senior Thesis

George Funkenbusch

Supervised by Professor Michael Giacomelli

Contents

1 Abstract

Due to their ease of use, manufacturability, and superior imaging speed/signal-to-noise ratio (SNR), Silicon Photomultipliers (SiPM) are becoming attractive alternatives to Photomultiplier Tubes (PMTs) for low-signal and single photon applications such as fluorescence microscopy and LiDAR [1]. However, SiPM-based detectors still have not been pushed to their maximum potential due to non-optimal readout electronics. For future directions in our lab, as well as viability of SiPM detectors for other high-speed applications, a higher bandwidth is desirable. In this report, we lay out the design process for our SiPM detector printed circuit board (PCB), the optimization of its electronics, and performance characterization. Through optimization of the circuit, we were able to achieve a maximum bandwidth of 315 MHz.

2 Background

2.1 Silicon Photomultiplier Principles

2.1.1 Single Photon Avalanche Diodes (SPADs)

SPADs are the building blocks of SiPMs. They are PIN photodiodes placed at a high reverse bias voltage, putting them in a region known as "Geiger mode." This is distinct from avalanche mode in that in Geiger mode in addition to electrons, holes are also accelerated enough to create additional hole-electron pairs. Unlike a PIN in avalanche mode, this process is self-sustaining and must be quenched by an external circuit (**Figure 1**). The sudden increase in current in response to a photon allows a SPAD to accurately determine the arrival of the photon. After firing, a SPAD has a long dead time due to quenching time and a recharging of the bias voltage. For this reason, singular SPADs are not suitable for fast imaging applications and a SiPM is necessary [6].

2.1.2 SPADs in Array

SiPMS are made up of thousands of SPADs connected in parallel. By placing this array at the Fourier plane of a system instead of the focus, one can circumvent the issue of an individual SPAD's downtime. The charge output by a SiPM is linearly proportional to the number of SPADs fired, making SiPMs

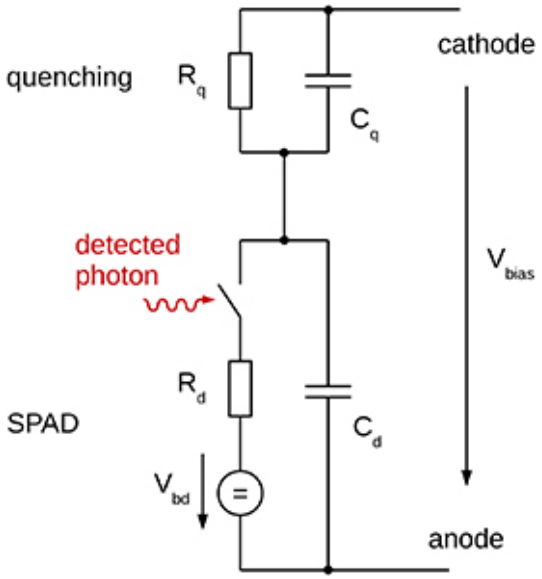

Figure 1: Equivalent electrical circuit model of a single photon avalanche diode (SPAD) [6]

well-suited to photon counting applications [5]. This parallel arrangement of SiPMS causes parasitic capacitances to appear in the circuit. Due to the complexity of the system, the exact effect of this parallel array is unknown. These capacitances contribute to a low-pass filter which may cause a hard limit to the possible achievable bandwidth. However, with current SiPM detector models the bandwidth is likely limited by either the gain-bandwidth of the op-amp used or the long tail of the SPAD response.

SiPMs improve upon many of PMTs' shortcomings. Notably, since SiPMs do not require a vacuum tube to operate, they are significantly cheaper, manufacturable, and easier to use than PMTs. In addition, since they are more durable they also have a higher saturation power than PMTs. This allows for higher signal powers to be used for certain applications, improving imaging speed/SNR. The gain mechanism in SiPMs is also determinstic rather than stochastic, affording additional improvements in SNR when compared to PMTs. One disadvantage of SiPMs compared to PMTs is the fill factor of 30%-80% depending on the size of the SiPM array [5]. However, this disadvantage is diminished by the improvement in quantum efficiency of the silicon photodiode when compared to PMT photocathode materials,

especially in the near-infrared range relevant to two-photon microscopy and LiDAR [3] (**Figure 2**).

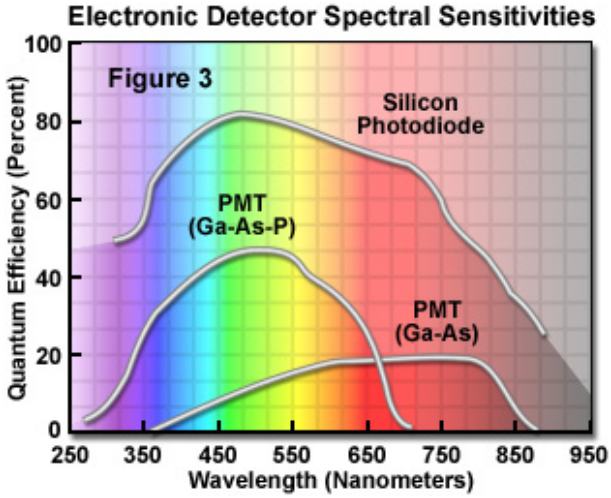

Figure 2: Quantum efficiency of silicon compared to some typical PMT photocathode materials. Note the improvement in the 650-850 nm region [3].

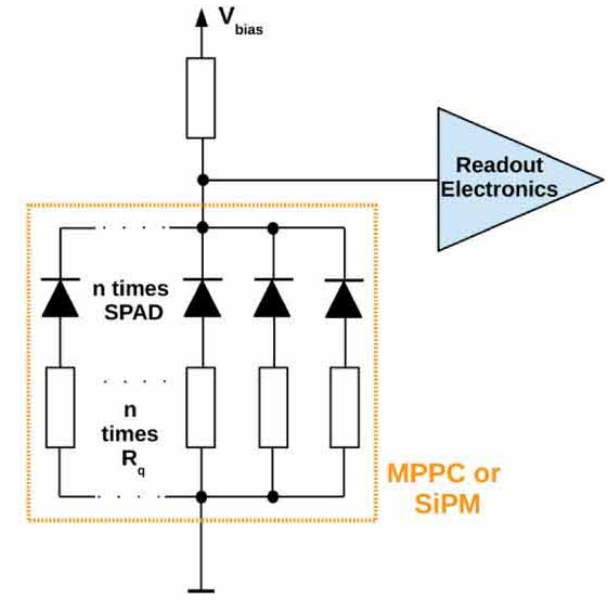

Figure 3: Schematic of an SiPM made up of n SPADs in parallel [6].

2.1.3 Detection Response

The photon response of a SiPM typically exhibits an extremely fast rise time on the order of a couple of nanoseconds followed by a slow decay time caused by the recharging bias voltage in a fired SPAD. This long "tail" is on the order of tens of nanoseconds and can cause issues in a variety of high-speed applications. For example, in point-scanning fluorescence microscopy it can limit the scanning speed of the system due to the signal from one pixel bleeding into the next [1]. In PET, if the tail of one photon arrival bleeds into the next photon arrival, it will affect the measurement of the arrival time by displacing the threshold [2].

In addition to the recharge time of individual SPADs, the bandwidth is also limited to a lesser extent by the readout electronics. There are three primary factors that influence the bandwidth: (1) the gain-bandwidth of the op-amp used, (2) the RC constant of the SiPM and readout electronics, and (3) the parasitic capacitances of the SPADs in parallel that make up the SiPM. These three factors can be modelled as low-pass filters all at different frequencies.

2.2 Pole-Zero Cancellation

To shorten the response tail and improve the bandwidth of the system, a technique known as Pole-Zero Cancellation (PZC) is utilized. In the frequency domain, the recharge time can be interpreted as a low-pass filter dependent on the capacitance and resistance of the SPAD. PZC essentially cancels this filter by having an opposing filter at the same frequency and magnitude. In the time domain, this can be interpreted as having a signal proportional to the derivative of the input added to a signal proportional to the input itself to remove the long tail while also avoiding negative values (**Figure 4**) [2]. This can either be done with a capacitor and resistor in parallel [2], or by a current divider with an inductor to ground (**Figure 5**) [1].

In this case, we are using the inductor current divider in the current domain of the op-amp. Placing the filter in the current domain rather than the voltage domain of the op-amp removes the slow component of the input, allowing the op-amp to use its whole dynamic range to amplify the fast component (**Figure 5**) [1]. In addition, using an inductor to filter behaves better than using a capacitor-based filter at fast frequencies.

One major disadvantage of this approach is that the attenuation of the low frequency component lowers the overall signal a great deal. More attenuation leads to a shorter tail but less signal, so a trade-off must be made to gain more bandwidth. This loss in signal can be compensated for by adjusting the gain of the op-amp in the circuit. In addition, enough of the slow component must be kept to prevent the signal from being negative.

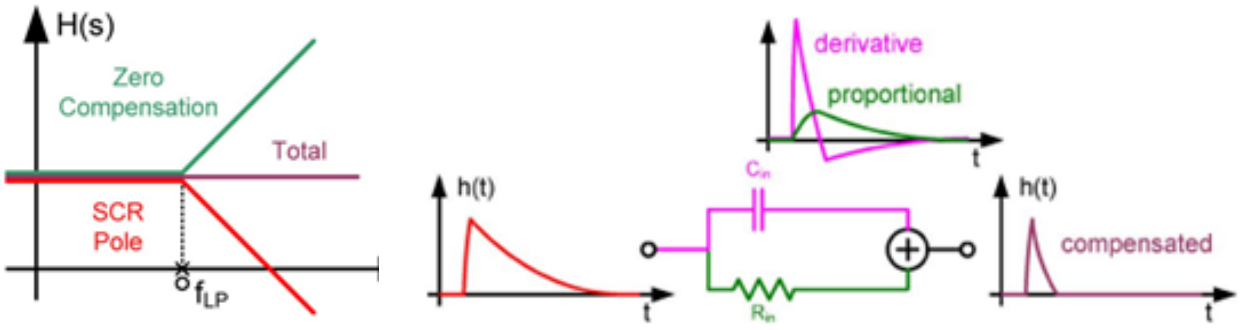

Figure 4: Frequency domain representation of PZC (left) and time domain representation of PZC (right) [2].

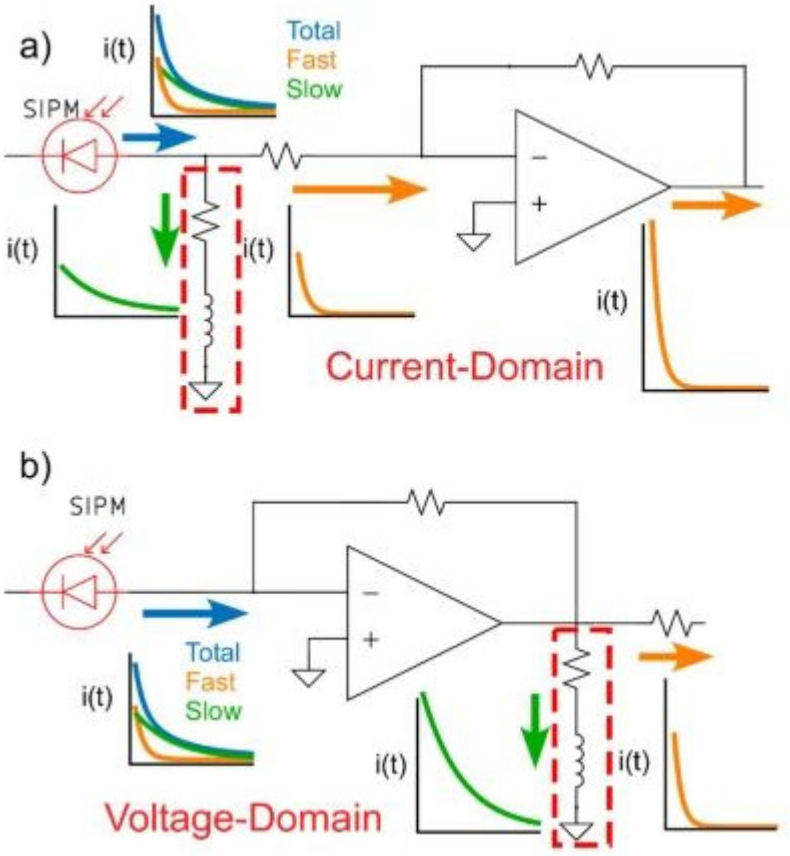

Figure 5: Example of inductor current divider PZC circuit in the (a) Current-Domain and (b) Voltage-Domain. [1]

2.3 High-Speed PCB Design

When working with high-speed circuits, additional factors should be taken into consideration for optimal performance. In high-speed PCBs, it is important to:

- Utilize bypass capacitors to prevent noise from supply rails
- Match transmission line impedances to components to prevent reflections

This section covers the basic design principles utilized to ensure good photodetector performance in our PCB.

2.3.1 Decoupling Capacitors

In high-frequency applications, high frequency noise from either the power source or other components connected to the same power rail can cause issues in the operation of the circuit. To prevent this noise, a decoupling capacitor is connected to ground to remove AC components.

Conceptually, the decoupling capacitor works by becoming a "battery" for the component it is attached to. Once it is charged, it can respond to ripples in the supplied voltage by quickly supplying power to the component in the case of a voltage drop or absorbing power in the case of a voltage spike. To suppress ripple across a broad band of frequencies, multiple decoupling capacitors of different capacitances are often placed in parallel [4].

One additional consideration is the placement of the bypass capacitors. Bypass capacitors should be placed as close as possible to the component they are supplying power so that the connection is a short circuit. This is especially important for smaller capacitors that are filtering high-frequency noise. When placing decoupling capacitors in parallel, it is common practice to place the smaller capacitors closer to the component [4]. In addition, bypass capacitors and transmission lines should be placed so that the overall loop formed by a supply to ground should be minimized. This is because the change in magnetic field according to Faraday's law scales with the area enclosed by the loop. Having a larger loop will increase the response time of the circuit to voltage ripple because more time is needed to allow for the magnetic field to change.

2.3.2 Impedance Matching

Just like discontinuities in the refractive index in a single-mode fiber cause reflection, so do discontinuities in the impedance of a circuit. The reflection coefficient is given by the following formula:

$$\Gamma = \frac{Z_2 - Z_1}{Z_2 + Z_1}$$

Transmission lines have an inherent impedance dependent on multiple factors including the width, height, dielectric constant, etc. In order to prevent signal reflections, the width of a transmission line must be adjusted to match the impedance of the source it is connected to.

3 Methods

3.1 PCB Design

Our PCB was designed using the open source software KiCad 6.0. The design was built upon a previous iteration, with special attention devoted to the position of decoupling capacitors and impedance matching. This new iteration replaces the Texas Instruments OPA847 op-amp with the newer OPA855, which has more than twice the gain-bandwidth.

The final design is shown in **Figure 6**. The loop area of the decoupling capacitor modules (highlighted in dark blue) are minimized. The size of the transmission line from R1 to J2 is impedance matched to the 50 ohm load resistor.

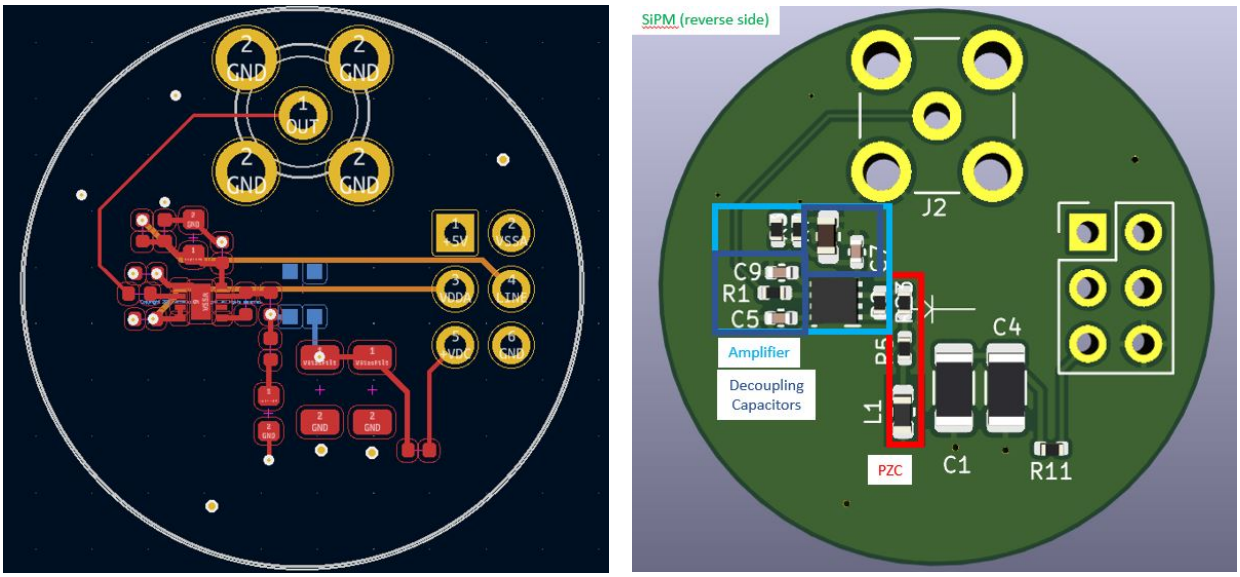

Figure 6: PCB design in KiCAD (left). Front transmission lines in red, back in blue, power layer in gold. CAD model of PCB in KiCAD (right). Hamamatsu S14160 SiPM mounted on reverse side.

3.2 PZC Electronics Optimization

A basic schematic of the PZC circuit is shown in **Figure 8**. The ratio of R1 and R2 controls how strong the PZC filter is, while the value of L1 controls the

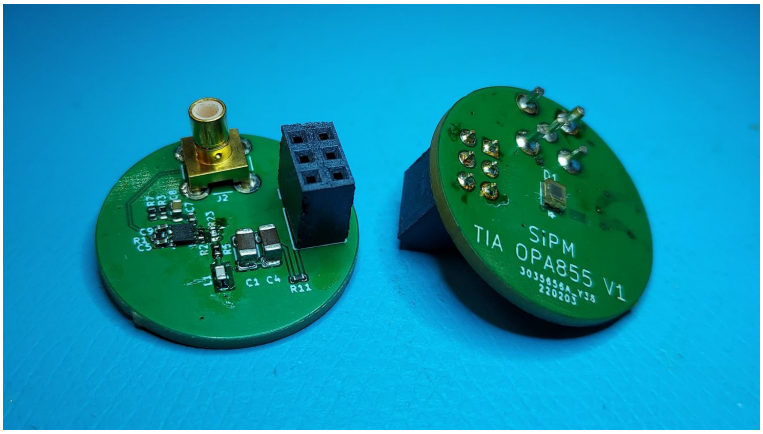

Figure 7: Assembled detector module. PCB is designed to fit in a 1 inch lens tube for ease of alignment.

frequency at which the PZC starts. By inspecting the shot noise spectrum, one can get a coarse understanding of how the resistors and inductors in the circuit should be adjusted to optimize the bandwidth and achieve the flattest frequency response possible.

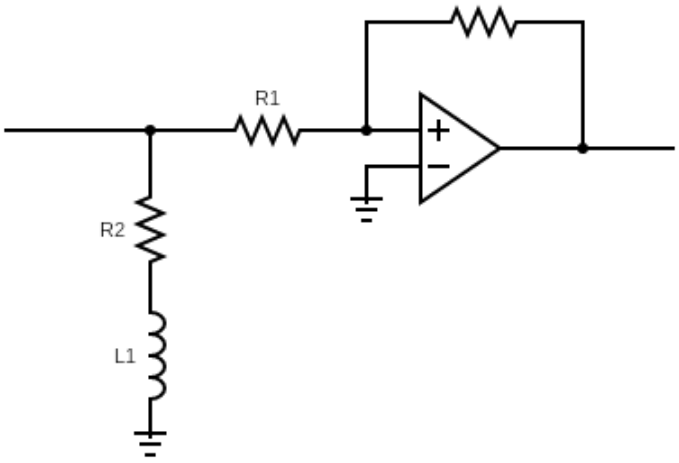

Figure 8: A basic schematic of the PZC circuit.

3.3 Performance Characterization

3.3.1 Shot Noise Power Spectrum

The bandwidth of the detector can be characterized using a Spectrum Analyzer. Performance is determined using the 3dB bandwidth of the detector, where the response falls to halfway between the peak and minimum values.

For comparison, this characterization was performed on both our optimized detector as well as a detector without the PZC circuit.

3.3.2 Time-Domain Impulse Response

In addition to characterizing the frequency domain response, it is also important for us to examine the time-domain impulse response. Phase imparted in the frequency spectrum may distort the time-domain response, causing ripples or stretching of the impulse response.

The setup consists of a MenloSystems YLMO Femtosecond Ytterbium Laser aimed at our photodetector. Since the pulse width of the laser is significantly shorter than our detector response time, it will appear approximately as a delta function to the detector, allowing us to measure the impulse response. Using a fast oscilloscope and heavily attenuating the laser incident on our detector, we were able to measure the detector's response to an impulse. Measurements for the detector without the PZC circuit could not be obtained, due to the laser's repetition rate of 100 MHz. The time between pulses was shorter than the decay time of the no-PZC detector, prohibiting accurate measurement.

4 Results

4.1 Shot Noise Power Spectrum

The shot noise power spectrum of our highest performing circuit so far is shown in **Figure 9**. The 3dB bandwidth is roughly 315 MHz. This is significantly higher than our previously published SiPM photodetector's 3dB bandwidth of 60 MHz [1]. For comparison, the shot noise power spectrum of a detector without the PZC circuit is shown in **Figure 10**. The 3dB bandwidth is roughly 18.33 MHz, significantly worse than our optimized circuit.

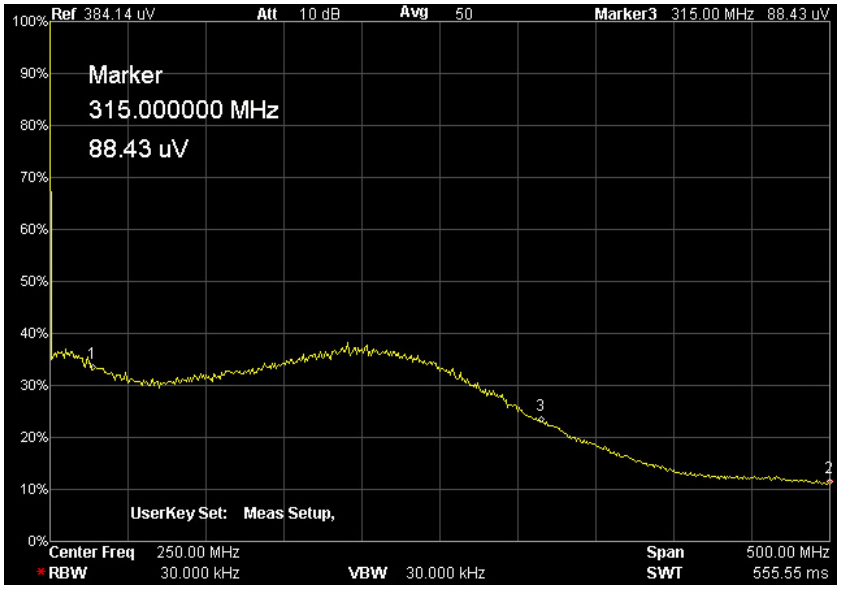

Figure 9: Shot noise power spectrum of highest bandwidth achieved photodetector. The 3dB bandwidth is approximately 315 MHz.

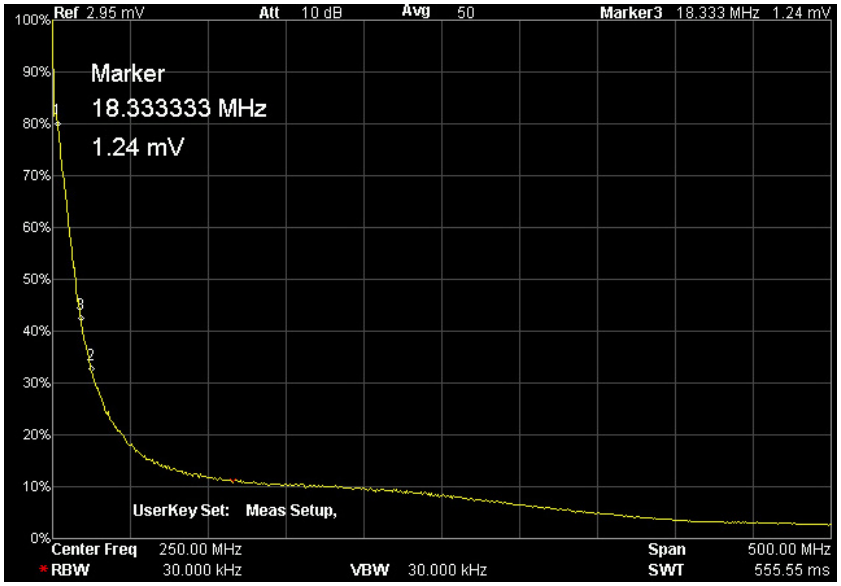

Figure 10: Shot noise power spectrum of detector with no PZC circuit. The 3dB bandwidth is approximately 18.33 MHz.

Our initial expectation was that if the PZC was properly balanced, our bandwidth would be limited by the gain-bandwidth of the op-amp. However, even with a well corrected frequency response curve, we were attaining values well below our expected op-amp bandwidth. We believe this is caused by the RLC time constant formed by the SiPM capacitance charging through the resistance and inductance of the PZC filter. This theory is supported by the fact that scaling the value of every component in the PZC circuit down allowed a further increase in bandwidth. However, further investigation will be necessary to confirm it.

4.2 Time-Domain Impulse Response

The measured time-domain impulse response is shown below in **Figure 11**. We estimated a FWHM of 1.7 ns and a 90-10 fall time of 1.5 ns.
For a bandwidth of 315 MHz, the 90-10 fall time should be 1.1 ns. This discrepancy is likely due to the curve in **Figure 9** not being flat. Further correction should be performed to flatten the curve and improve the impulse response. However, due to time limitations and the components available on-hand, this correction will have to take place in the future.

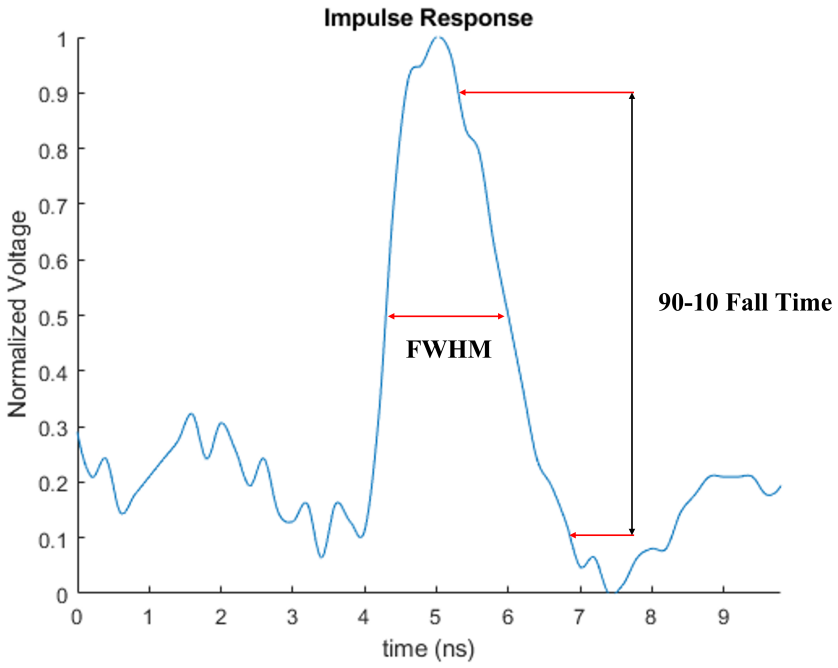

Figure 11: Time domain impulse response of the optimized photodetector. FWHM estimated to be 1.7 ns, 90-10 fall time estimated to be 1.5 ns.

5 Conclusion and Future Direction

By replacing the op-amp and optimizing the PZC circuit, we were able to achieve an increase in the 3dB bandwidth from approximately 60 MHz to 315 MHz. Our success in improving the bandwidth shows great potential for SiPMs for various high-speed applications including LiDAR and point-scanning fluorescence microscopy.

In the future, we will aim to improve the impulse response by flattening the shot noise power spectrum curve and further scaling down the overall impedance of the components in the PZC circuit. Additional characterization of the photodetector should also be performed, including plotting the photon transfer curve to investigate the dynamic range of the detector. In addition, we believe that better characterization of the impulse response can potentially take place with a lower repetition rate pico or femtosecond laser to allow more time for impulse responses to decay between samples.

6 Acknowledgements

I would like to thank my principal investigator, Professor Giacomelli, as well as his graduate students Vincent Ching-Roa, Chi Huang, and Yihan Liu for welcoming me into their lab and supporting my endeavors. I also want to thank Professors Andrew Berger, Julie Bentley, Jim Zavislan, and Jen Kruschwitz for their support and advice throughout my time as an undergraduate. Finally, I would like to acknowledge Professor Knox for organizing the Senior Thesis course.

7 Advisor Approval

Michael Giacomelli
to me ▾

I approve!

--
Michael Giacomelli, Ph.D.
Assistant Professor
Department of Biomedical Engineering & Institute of Optics
University of Rochester

References

[1] Ching-Roa, Vincent et al. "Ultrahigh-speed point scanning two-photon microscopy using high dynamic range silicon photomultipliers". In: *Scientific Reports* 11.5248 (2021). DOI: https://doi.org/10.1038/s41598-021-84522-0.

[2] Gola, Alberto et al. "Analog circuit for timing measurements with large area SiPMs coupled to LYSO crystals". In: *2011 IEEE Nuclear Science Symposium Conference Record* (2011), pp. 725–731. DOI: 10.1109/NSSMIC.2011.6154091.

[3] Spring Kenneth and Michael Davidson. *Electronic Imaging Detectors*. URL: https://hamamatsu.magnet.fsu.edu/articles/digitalimagingdetectors.html.

[4] M. Abu Khater. "High-Speed Printed Circuit Boards: A Tutorial". In: *IEEE Circuits and Systems Magazine* 20.3 (thirdquarter 2020), pp. 34–45. DOI: 10.1109/MCAS.2020.3005484.

[5] Piatek Slawomir. *What is an SiPM and how does it work?* URL: https://hub.hamamatsu.com/jp/en/technical-note/how-sipm-works/index.html.

[6] Gundaker Stefan and Arjan Heering. "The silicon photomultiplier: fundamentals and applications of a modern solid-state photon detector". In: *Physics in Medicine & Biology* 65.17 (2020).